arXiv:0807.4939v1 [nucl-th] 30 Jul 2008

Coalescence Models For Hadron Formation From Quark Gluon Plasma

RAINER FRIES[1,2] (RJFRIES@COMP.TAMU.EDU)

VINCENZO GRECO[3,4] (GRECO@LNS.INFN.IT)

PAUL SORENSEN[5] (PRSORENSEN@BNL.GOV)

[1]*Texas A&M University, College Station, Texas,*

[2] *RIKEN/BNL Research Center, Upton, New York,*

[3]*Istituto Nazionale di Fisica Nucleare –INFN-LNS, Catania, Italy,*

[4]*Department of Physics and Astronomy, University of Catania, Italy*

[5]*Brookhaven National Laboratory, Upton, New York*

Key Words quark gluon plasma, recombination, coalescence, hadronization, elliptic flow, heavy-ion collisions

Abstract We review hadron formation from a deconfined quark gluon plasma (QGP) via coalescence or recombination of quarks and gluons. We discuss the abundant experimental evidence for coalescence from the Relativistic Heavy Ion Collider (RHIC) and compare the various coalescence models advocated in the literature. We comment on the underlying assumptions and remaining challenges as well as the merits of the models. We conclude with a discussion of some recent developments in the field.

CONTENTS

1   Introduction

Collisions between heavy nuclei are used to probe the properties of nuclear matter at high temperature and density. Lattice QCD calculations indicate that if nuclear matter is heated above a critical temperature $T_c \approx 185$ MeV, quark and gluon degrees of freedom will be liberated and a deconfined quark-gluon plasma (QGP) forms (1, 2). Unambiguous signatures of quark gluon plasma formation in heavy-ion collisions have been sought for decades. Recently, experiments at the Relativistic Heavy Ion Collider (RHIC) have presented evidence that such a new state of matter has finally been found in collisions of Au atoms at a center of mass energy of $\sqrt{s} = 200$ GeV per nucleon-nucleon pair (3, 4).

The hot QGP phase formed in nuclear collisions at RHIC with a core temperature in excess of 300 MeV only lasts for an extremely short time. It quickly expands due to the large pressure and cools on the way. Eventually, the quark and gluon constituents need to combine into color-neutral objects and hadrons have to be formed when the temperature reaches T_c. The process of hadronization from a QGP may be quite different from hadronization in other cases, such as hadronization of hard scattered parton in elementary collisions where no thermalization is reached and no bulk of partons is formed. In this review we discuss a model of QGP hadronization by coalescence or recombination of quarks and gluons. The models discussed here have had success in describing many salient features of hadron production in heavy-ion collisions.

The emergence of recombination models was largely motivated by several unexpected observations (3) which were discussed as "the baryon puzzle" for a while. This was referring to measurements of baryon production in the intermediate transverse momentum region ($1.5 < p_T < 5$ GeV/c) (5, 6). Both the yield and

the elliptic flow of baryons exhibited strange features. In nucleon-nucleon colli-

sions at $p_T = 3$ GeV/c, only one baryon is produced for every three mesons (1:3),

reflecting the larger mass and the requirement of a non-zero baryon number to

form the baryon. In Au+Au collisions at RHIC however, baryons and mesons are

created in nearly equal proportion (1:1) despite those differences. In the same

p_T-region, the elliptic anisotropy (v_2) of baryons is also 50% larger than that for

mesons. Therefore, baryon production is particularly enhanced in the direction

of the impact vector between the colliding nuclei (in-plane) (6, 7).

The large baryon v_2 eliminates several possible alternative solutions put for-

ward for the baryon puzzle. The most common explanations for the baryon

anomaly at RHIC were

- *coalescence or recombination* — Multi-quark or gluon processes during
  hadron formation (8, 9, 10, 11, 12).

- *baryon junctions* — Gluon configurations that carry baryon number (13).

- *flow* — Collective motion that populates the higher p_T-regions of phase
  space for the more massive baryons, as described by hydrodynamics (14,
  15, 16).

Only coalescence models have survived the tests imposed by an impressive amount

of data taken after the original discovery of the baryon enhancement. They are

particularly attractive because they seem to provide a natural explanation for the

valence quark-number scaling that has been observed in v_2 measurements. They

also relate hadronic observables to a pre-hadronic stage of interacting quarks

and gluons. As such, they touch on questions central to the heavy-ion physics

program: deconfinement and chiral symmetry restoration.

This review is organized as follows. In the remainder of this section we discuss

the general context of hadronization and a brief history of recombination models. We also review the experimental evidence from RHIC. In Sec. 2 we review the basic theory and compare the different implementations of recombination models. In Sec. 3 we present a comprehensive overview of the available data which can be addressed by coalescence. We conclude with a discussion of open questions, recent developments and future directions of research in Sec. 4.

1.1 Hadronization

Hadronization has always been a challenging aspect of quantum chromodynamics (QCD), the fundamental theory of the strong force. QCD bound-states are non-perturbative in nature and a first-principle description of their formation has yet to be obtained. In this subsection we briefly discuss two approaches to deal with hadronization which are routinely used in nuclear and particle physics; both of them have connections to the recombination model discussed in this review.

Light cone wave functions are used to describe the structure of hadrons relevant for exclusive processes (17). Exclusive here means that they deal with a full set of partons with the quantum numbers of the hadron. Exclusive processes at high momentum transfer are naturally dominated by the few lowest Fock states. Formally, light cone wave functions are matrix elements of the set of parton operators between the vacuum and the hadron state in the infinite momentum frame, e.g. $\phi_p \sim \langle 0|uud|p \rangle$, schematically, for a proton p. They describe the decomposition of the hadron in longitudinal momentum space in terms of partons with momentum fractions x_i. From theory these wave functions are only constrained by very general arguments like Lorentz-covariance and approximate conformal symmetry. Direct measurements are difficult, but estimates have become available in recent

years, in particular for the lowest Fock state of the pion (18, 19).

A complementary technique has been developed for inclusive hadron production, *initial state* $\to h + X$, at large momentum transfers in which a single colored parton a has to hadronize into the hadron h. For this purpose fragmentation or "parton decay" functions $D_{a \to h}(z)$ have been defined (20). They give the probability to find the hadron h in parton a with a momentum fraction z, $0 < z < 1$. The cross section for inclusive hadron production in $e^+ + e^-$, lepton-hadron or hadron-hadron collisions can then be written as a convolution

$$\sigma_H = \sigma_a \otimes D_{a \to h} \tag{1}$$

of the production cross section σ_a for parton a with the fragmentation function $D_{a \to h}(z)$ (21, 22). Fragmentation functions are not calculable in a reliable way from first principles in QCD. However, they are observables and can be measured experimentally. Parameterizations using data mostly from $e^+ + e^-$ collisions are available from several groups (23). Physically, the fragmentation of a single parton happens through the the creation of $q\bar{q}$ pairs (through string breaking or gluon radiation and splitting) which subsequently arrange into color singlets, and eventually form hadrons.

Both examples above apply to processes with a large momentum transfer, i.e. with a perturbative scale $\mu \gg \Lambda_{\mathrm{QCD}}$. They are based on the concept of QCD factorization which separates the long and short distance dynamics.[1] Such a perturbative scale is absent for the hadronizing bulk of partons in a heavy ion collision and neither technique, fragmentation nor exclusive wave functions, can

---

[1]Note that we have neglected the scale dependence in the notation for wave functions and fragmentation functions for simplicity. A discussion of the scale dependence can be found in the original references given.

be readily applied in this situation.

To see the challenge more clearly, let us compare the different initial conditions for the hadronization process. Fragmentation applies to a single parton in the vacuum, whereas exclusive wave functions are applied to a full set of valence quarks in the vacuum. On the other hand, the initial state just before hadronization in nuclear collisions is a thermal ensemble of partons just above T_c. The exact degree of thermalization is not clear a priori, but we will see below, that complete thermalization might not be necessary.

Rather, the crucial point seems to be that partons have a certain abundance in phase space such that there is no need for the creation of additional partons through splitting or string breaking. The most naive expectation for such a scenario is a simple recombination of the deconfined partons into bound states. Indeed, there is experimental evidence that this is the correct picture for hadronization even long before a thermal occupation of parton phase space is reached.

1.2   Early Approaches to Recombination

Recombination models have first been suggested shortly after the invention of QCD in the 1970s. They successfully described hadron production in the very forward region of hadronic collisions (24). The observed relative abundances of hadrons clearly deviate from expectations from fragmentation in this region. This is known as the leading particle effect (25). E.g. a clear asymmetry between D^- and D^+ mesons was found in fixed target experiments with π^- beams on nuclei by the FNAL E791 collaboration (26). The measured D^-/D^+ asymmetry goes to 1 in the very forward direction, while fragmentation predicts that this asymmetry is very close to 0. This result can be explained by recombination of the $\bar{c}$ from a $c\bar{c}$

pair produced in the collision with a d valence quark from the beam π^- remnants. This mechanism is enhanced compared to the $c+\bar{d}$ recombination which involves only a sea quark from the π^- (27). There is no thermalized parton phase in this example, which strongly backs our argument at the end of the last subsection.

We are led to the important conclusion that the presence of any reservoir of partons leads to significant changes in hadronization. Vacuum fragmentation is no longer a valid picture in this situation. The reservoir of partons in the case of the leading particle effect is the soft debris from the broken beam hadron. In heavy ion collisions it is the distribution of thermal partons. First applications of the coalescence picture to nuclear collisions appeared in the early 1980s (28). This eventually led to the development of the ALCOR coalescence model in the 1990s (29, 30, 31). ALCOR focuses on hadron multiplicities and was successfully applied to hadron production at RHIC and the lower energies at the CERN SPS.

1.3 Challenges at RHIC

Results from the first years of RHIC triggered a revival for recombination models applied to heavy ion collisions in an unexpected region. Three measurements in particular, taken in the intermediate p_T range (1.5 GeV/c < p_T < 5 GeV/c), have defied all other explanations. This region is outside of what was thought to be the "bulk" of hadron production (p_T < 1.5 GeV/c) whose features should be described by thermalization and hydrodynamic collective motion (ALCOR describes bulk hadronization). Rather, the intermediate p_T region was expected to be dominated by fragmentation of QCD jets, after it was confirmed that this was the case for pion production in $p + p$ collisions at RHIC (32). However, the results from RHIC clearly pointed towards a strong deviation from the fragmen-

tation process at intermediate p_T in central Au+Au collisions. The three key observables were

- the enhanced baryon-to-meson ratios (5, 33).

- the nuclear modification factors R_{AA} and R_{CP} — *i.e.* the ratio of yields in central Au+Au collisions compared to peripheral Au+Au (R_{CP}) or $p + p$ (R_{AA}) collisions scaled by the number of binary nucleon-nucleon collisions (5, 6).

- the anisotropy of particle production in azimuthal angle relative to the reaction plane — *i.e.* the elliptic flow parameter v_2 (6, 35, 34, 7).

Fig. 1 shows the measured anti-proton/pion (5) and $\overline{\Lambda}/K_S^0$ (33) ratios as a function of p_T for various centralities and collision systems. At intermediate p_T, a striking difference is observed between the baryon-to-meson ratios in central Au+Au collisions and those in $e^+ + e^-$ (36) or $p + p$ collisions (37). The measurements in Fig. 1 indicate that the process by which partons are mapped onto hadrons are different in Au+Au collisions and in $p + p$ collisions. Changes solely to the parton distributions prior to hadronization are not likely to lead to such drastic changes in the relative abundances.

Fig. 2 shows the nuclear modification factor R_{CP} measured at RHIC for various identified hadrons. If the centrality dependence of particle yields scales with the number of binary nucleon-nucleon collisions, R_{CP} will equal one. A suppression at high p_T is taken as a signature for the quenching of jets in the bulk matter formed in central collisions. However, baryons ($\Lambda + \overline{\Lambda}$, $\Xi + \overline{\Xi}$, and $\Omega + \overline{\Omega}$) (33, 38) systematically show less suppression than mesons (kaons or ϕ) (39, 40)). The same behavior was found for protons and pions (41). This key result shows that the mass of a hadron is less important for its behavior at intermediate p_T than

the fact whether it has two or three valence quarks. This ruled out explanations blaming collective motion (flow) for the baryon enhancement, and it is a strong indication that parton degrees of freedom are important. Last doubts were erased by a direct comparison of protons and ϕ mesons which have the same mass but a different valence quark content: ϕ mesons behave like other, lighter mesons, not like protons (40, 42).

In non-central nucleus-nucleus collisions, the overlap region of the nuclei is elliptic in shape. Secondary interactions can convert this initial coordinate-space anisotropy into an azimuthal anisotropy of the final momentum-space distribution. That anisotropy is commonly expressed in terms of the coefficients from a Fourier expansion of the azimuthal dependence of the invariant yield (43), see Sec. 2. The second component (the "elliptic flow" parameter v_2) is large due to the elliptic shape of the overlap region. Fig. 3 shows the measured values for v_2 as a function of p_T for pions, kaons, protons and Lambda hyperons (6,35). In the bulk region ($p_T < 1.5$ GeV/c), v_2 is increasing with p_T (44). In this region the v_2 values for different hadrons are ordered by their mass with more massive particles having smaller v_2 values (6,35,45). This mass ordering is qualitatively understood in hydrodynamic models of the expansion of the bulk of the fireball (14). Some hydrodynamic calculations are also shown in the figure. For $p_T > 1.5$ GeV/c, the data clearly deviates from hydrodynamic calculations. The measured v_2 seems to saturate, as predicted by parton cascades (46), and the particle-type dependence reverses: v_2 values for the more massive baryons are larger than those for mesons.

v_2 can also be generated if jets are quenched in the quark gluon plasma (47). However, such calculations grossly underestimate the measured values of v_2, in particular when they simultaneously have to explain values of R_{CP} close to one.

The data clearly shows that although protons and hyperons have R_{CP} values near unity, their maximum v_2 values exceed those of pions and kaons by approximately 50%. Taken together, the particle-type dependence of v_2 and R_{CP} provide very stringent tests of various models for particle production and have ruled out pure jet fragmentation or simple hydrodynamics as models for hadron production at intermediate p_T.

2 Formulations of Hadronization by Recombination

2.1 Basic Theory

Coalescence or recombination of particles is a very general process that occurs in a wide array of systems from the femtometer scale to astrophysics. In all these fields a first approach is to discard the details of the dynamical process in favor of exploiting an adiabatic approximation in which a projection of the initial state onto the final clusterized state is considered. In the specific case of recombination of partons, most work found in the literature uses an instantaneous projection of parton states onto hadron states. The expected number of hadrons h from a partonic system characterized by a density matrix ρ is given by

$$N_h = \int \frac{d^3 P}{(2\pi)^3} \left\langle h; \mathbf{P} \right| \rho \left| h; \mathbf{P} \right\rangle . \tag{2}$$

Instantaneous here means that the states are defined on a hypersurface which is typically either taken to be at constant time, $t = \text{const.}$, or on the light-cone $t = \pm z$. In this case information about the hadron bound state is schematically encoded in a wave function or Wigner function. As we will see this approach leads to very simple math, but it has the conceptual disadvantage that only three components of the four momentum are conserved in such a $2 \to 1$ or $3 \to 1$

coalescence process. A more dynamical approach based on resonance scattering can be realized, which avoids this problem (48). The information about the hadron bound state is then encoded in a cross section. In this section, we will focus on the instantaneous projection formalism which has had great success explaining RHIC data. We will come back to the dynamic formulation in Sec. 4.

All available models of instantaneous coalescence can be traced back to the following basic formula which can be derived from Eq. (2). The number of mesons with a certain momentum $\mathbf{P}$ is (49)

$$\frac{dN_M}{d^3P} = \sum_{a,b} \int \frac{d^3R}{(2\pi)^3} \frac{d^3q\,d^3r}{(2\pi)^3} W_{ab}\left(\mathbf{R} - \frac{\mathbf{r}}{2}, \frac{\mathbf{P}}{2} - \mathbf{q}; \mathbf{R} + \frac{\mathbf{r}}{2}, \frac{\mathbf{P}}{2} + \mathbf{q}\right) \Phi_M(\mathbf{r}, \mathbf{q}). \quad (3)$$

Here M denotes the meson and a, b are its coalescing valence partons. W_{ab} and Φ_M are the Wigner functions of the partons and the meson respectively, $\mathbf{P}$ and $\mathbf{R}$ are the momentum and spatial coordinate of the meson, and $\mathbf{q}$ and $\mathbf{r}$ are related to the relative momentum and position of the quarks. The sum runs over all possible combinations of quantum numbers of the quarks in the hadron, essentially leading to a degeneracy factor C_M.

Note that coalescence, just as its counterpart in exclusive processes, is based on the assumption of valence quark dominance, i.e. the lowest Fock states are the most important ones. The corresponding formula for baryons containing 3 valence quarks can easily be written down as well. It is also straightforward to generalize Eq. (3) to include more partons which would be gluons or pairs of sea quarks, accounting for the next terms in a Fock expansion (51).

For a meson consisting of two quarks its Wigner function is formally defined as

$$\Phi_M(\mathbf{r}, \mathbf{q}) = \int d^3s\, e^{-i\mathbf{s}\cdot\mathbf{q}} \varphi_M\left(\mathbf{r} + \frac{\mathbf{s}}{2}\right) \varphi_M^*\left(\mathbf{r} - \frac{\mathbf{s}}{2}\right) \quad (4)$$

where the 2-quark meson wave function in position space φ_M can be represented

as

$$\langle \mathbf{r}_1; \mathbf{r}_2 | M; \mathbf{P} \rangle = e^{-i\mathbf{P}\cdot(\mathbf{r}_1+\mathbf{r}_2)/2} \varphi_M (\mathbf{r}_1 - \mathbf{r}_2) \tag{5}$$

The Wigner function of the partons can be defined in a similar way from the density matrix ρ (49).

To evaluate Eq. (3) expressions for the hadron wave functions and for the distribution of partons have to be used as input. We discuss the different implementations in the next subsection. Let us emphasize two common features of all implementations. For one, the Wigner function for the multi-parton distribution is usually approximated by its classical counterpart, the phase space distribution of the partons on the hypersurface of hadronization. Secondly, Eq. (3) is made explicitly Lorentz-covariant to account for the relativistic kinematics.

2.2 Different Implementations of Recombination

Different manifestations of Eq. (3) have been used in the literature (52). Closest to the master formula is the implementation by Greco, Ko and Lévai [GKL] (11, 53). In this approach the full overlap integral in Eq. (3) over both relative position and momentum of the partons is calculated. On the other hand, several groups, (e.g. Fries, Müller, Nonaka and Bass [FMNB] (10, 49, 50); Hwa and Yang [HY] (54, 55) and Rapp and Shuryak [RS] (56) simplify the situation by integrating out the information about position space. This leads to a formulation solely in momentum space in which the information about the hadron is further compressed into a squared (momentum space) wave function (also called a recombination function by some authors).

The implementation by Greco, Ko and Lévai was originally motivated by a relativistic extension of the formalism for the coalescence of nucleons into deuterons

and other light clusters in relativistic heavy-ion collisions. Coalescence has been successfully applied to nucleons for more than two decades (57, 58). GKL use a manifestly covariant version of Eq. (3) for the number of mesons coalescing

$$N_M = C_M \int \prod_{i=a,b} (p \cdot d\sigma)_i \, d^4 p_i \, \delta(p_i^2 - m_i^2) W_{ab}(r_a, p_b; r_b, p_b) \Phi_M(r; q) \,. \quad (6)$$

The relative phase space coordinates $r = r_b - r_a$ and $q = p_b - p_a$ are the four-vector versions of the vectors $\mathbf{r}$ and $\mathbf{q}$ in Eq. (3). $d\sigma$ is a volume element of a space-like hypersurface. The hypersurface of coalescing partons is usually fixed by GKL through the condition of equal longitudinal proper time $\tau = \sqrt{t^2 - z^2}$.

In the GKL formalism the full phase space overlap of the coalescing particles is calculated. For mesons this leads to a 6-dimensional phase space integral which is computed using Monte-Carlo techniques (53). This has the advantage to avoid some of the more restrictive approximations employed by other groups. In addition, the numerical implementation of the 6D-phase space integral can be applied directly to a quark phase which has been extracted from a realistic dynamic modeling of the phase space evolution in the collision. Soon after the first implementation of GKL, similar techniques were used for hadronization in the partonic cascade approach by Molnar (59).

The hadron Wigner function for light quarks used by GKL is a simple product of spheres in position and momentum space

$$\Phi_M(r; q) = \frac{9\pi}{2} \Theta \left[\Delta_r^2 - r^2 \right] \times \Theta \left[\Delta_p^2 - q^2 + (m_1 - m_2)^2 \right] \,. \quad (7)$$

The radii Δ_r and Δ_p in the Wigner formalism obey the relation $\Delta_p = \Delta_r^{-1}$, motivated by the uncertainty principle. The parameter Δ_p is taken to be different for baryons and mesons and is of the order of the Fermi momentum. Gaussian Wigner functions are used if heavy quarks are involved (60) (see also Fig. 9).

The Wigner functions used in the GKL approach appear to be more arbitrary then those based on light cone wave functions (see FMNB below) However, it turns out that many aspects of coalescence do not depend critically on the wave function for systems close to thermalization. On the other hand, using the full information about the phase space distribution of partons permits a direct connection to many quantitative properties of the bulk of the fireball, like the multiplicity of partons, and the energy and entropy densities just before hadronization. The parameters found by GKL in order to reproduce the behavior of hadron spectra at intermediate p_T also provide a bulk of the partonic fireball which is consistent with what can be inferred from hydrodynamics and experimental data. E.g., the radial flow, parameterized as $\beta = \beta_0 r/R$ exhibits a slope parameter $\beta_0 = 0.5$ consistent with hydrodynamical calculations at the end of the quark-gluon plasma phase (15). Moreover the energy density at hadronization is $\epsilon = 0.8$ GeV/fm^3, which is very close to what is expected from lattice QCD calculations (1, 2). In addition, the entropy is found to be $dS/dy \approx 4800$ in agreement with the value inferred from experimental data by Pratt and Pal (61).

Compared to the full phase space implementation which is rather complex, simplified momentum space models focus on a direct exposition of some key features which can then be treated analytically. We will discuss the implementation by Fries, Müller, Nonaka and Bass in detail here, but the approaches taken by Hwa and Yang, and Rapp and Shuryak are very similar.

The first assumption made by FMNB is that variations in the quark distribution across the size of a pre-hadronic state (which may be smaller than a free hadron) are small. The integration over the relative position of the quarks can then be carried out. For further simplification one focuses on the case that the

momentum $|\mathbf{P}|$ of the hadron is much larger than the mass M. This allows one to treat the hadron as being on the light cone with a large $+$-momentum, $P^+ \gg P^-$ (the z-axis in the lab frame is here taken to point into the direction of the hadron; this is called the hadron light cone frame in (49)). The momenta of the partons inside the hadron can be parameterized by light cone fractions x_i of P^+ ($0 < x_i < 1$) and transverse momenta $\mathbf{k}_i$ orthogonal to the hadron momentum $\mathbf{P}$. The momenta $\mathbf{k}_i$ are usually integrated as well in a trivial way, leaving a single longitudinal momentum integration.

In the absence of any perturbative scale the light cone wave functions are not known from first principles. But, again, the coalescence from partons thermally distributed in phase space is not very sensitive to the shape of the wave functions. For the lowest Fock state of a meson the squared wave function or recombination function is usually parameterized as (49)

$$\Phi_M(x_1, x_2) = B x_1^{\alpha_1} x_2^{\alpha_2} \delta(x_1 + x_2 - 1) \,. \tag{8}$$

Here the α_i are powers which determine the shape, and the constant B is fixed to normalize the integral over Φ_M to unity. The yield of mesons with momentum P can then be expressed as

$$\frac{dN_M}{d^3P} = C_M \int_\Sigma \frac{d\sigma \cdot \mathbf{P}}{(2\pi)^3} \int_0^1 dx_1 dx_2 \Phi_M(x_1, x_2) W_{ab}(x_1 \mathbf{P}; x_2 \mathbf{P}) \tag{9}$$

where $d\sigma$ is the hypersurface of hadronization. In many cases the emission integral over the hypersurface is not calculated explicitly, but replaced by a normalization factor proportional to the volume of the hadronization hypersurface.

Several choices for the powers α_i can be found in the literature. Asymptotic light cone distribution amplitudes suggest $\alpha_i = 2$ for light valence quarks. For heavy-light mesons the relative size of the powers has to be adjusted such that the

average velocity of the quarks is about the same. E.g. for a charm and light quark system, like the D meson, values $\alpha_c = 5$, $\alpha_{u,d} = 1$ are used by Rapp and Shuryak (56). It is sometimes useful to look at the extreme case $\alpha_i \to \infty$ with the ratio of the α_i fixed. For two light quarks this implies $\Phi_M(x_1, x_2) = \delta(x_1 - 1/2)\delta(x_2 - 1/2)$. This is the limit of a very narrow wave function in momentum space and the remaining integral is trivial.

Analytic implementations of recombination applied to intermediate p_T in heavy ion collisions usually assume a thermal distribution of partons at hadronization. For such a system it seems to be sufficient to neglect correlations between partons and to use a factorization into single-particle phase space distributions

$$W_{ab}(r_a, p_a; r_b, p_b) = f_a(r_a, p_a) f_b(r_b, p_b) \,. \tag{10}$$

With thermal one-particle distributions f this gives good results for single inclusive spectra, hadron ratios, etc. at RHIC. Observables dealing with correlations of hadrons are more sensitive to correlations among partons. Results from RHIC seem to suggest that jet-like correlations between bulk partons exist down to intermediate p_T and have to be taken into account (62). This will be addressed in more detail below. Coalescence applied to non-thermal systems, e.g. to parton showers (63, 64), or hadronic collisions (56), require more sophisticated models for multi-parton distributions.

As we have mentioned above, recombination of partons in a thermal ensemble has the interesting property that the process is largely independent of the shape of the hadron wave function. This can be most easily seen using the FMNB formalism with the partons coming from the tail of a Boltzmann distribution

$e^{-p/T}$. For a meson with large momentum P the integral in (9) is

$$\sim \int_0^1 dx_a dx_b \Phi_M(x_a, x_b) e^{-x_a P/T} e^{-x_b P/T} \sim e^{-P/T} \int_0^1 dx_a dx_b \Phi_M(x_a, x_b), \quad (11)$$

independent of the shape of Φ_M. Moving to lower hadron P_T or using the full phase-space overlap, as in GKL, make this argument less rigorous. But even in those cases the results are only weakly dependent of the shape of the wave function unless very extreme choices are made. From this small exercise we can read off another important fact, which is tantamount to solving the baryon puzzle at RHIC: both mesons and baryons would lead to the same Boltzmann distribution $\sim e^{-P/T}$ (for sufficiently large momentum P), which is very different from the suppression for baryons expected from fragmentation.

2.3 Competing Mechanisms of Hadron Production

In order to compute realistic hadron spectra that can be compared to data measured in heavy-ion collisions, other important mechanisms of hadron production have to be considered as well. QCD factorization theorems state that leading-twist hard parton scattering with fragmentation is the dominant mechanism of hadron production at asymptotically high momentum transfer (22). This can also be seen from the simple analytic formulas discussed in the previous subsection. Let us again consider the tail of a thermal parton distribution $f_{\text{th}} \sim A e^{-p/T}$ and compare it to a power-law distribution $f_{\text{jet}} \sim B p^{-\alpha}$ for large p. Power-law distributions are typical for partons coming from single hard scatterings. Both recombination and fragmentation preserve the basic shapes of the underlying parton distribution.

As we have already argued above, recombination of n thermal partons leads to a thermal distribution for the resulting hadrons with the same slope $\sim A^n e^{-p/T}$,

while the slope of a hadron recombining from n hard partons would steepen to $\sim B^\alpha p^{-n\alpha}$ (note that these n hard partons would come from n different jets!). On the other hand, fragmentation from a single hard parton just leads to a shift in the slope of the power law $\sim B p^{-\alpha-\delta}$. Given that $\alpha \approx 6 \ldots 8$ this suggests that recombination of hard partons is not an important mechanism, but that recombination is very efficient for thermal partons. On the other hand, the exponential suppression of the thermal spectrum will set it in at some value of p and lead to a power-law spectrum of hadrons from fragmentation off jets at very large p, in accordance with perturbative QCD.

Hence from very basic considerations we expect a transition from a domain dominated by recombination of thermal partons at intermediate p_T to a regime dominated by fragmentation of jets at very high p_T. It is also clear that this transition happens at higher values of p_T for baryons compared to mesons, since recombination produces baryons and mesons with roughly the same abundance, while baryons are suppressed in jet fragmentation.

This dual aspect of hadron production and the transition region are treated in different ways in the literature.

- In publications by the FMNB group thermal recombination is supplemented by a perturbative calculation including jet quenching and fragmentation. The two components of the spectrum are simply added (49). No mixing of the thermal and hard partons is included, leading to a rather sharp transition between the two regions.

- The GKL group allows coalescence between soft and hard partons as well. For mesons this would correspond to a term

$$\sim f_{\text{th}}(p_a) f_{\text{jet}}(p_b) \Phi_M(p_a - p_b) \,. \tag{12}$$

- A technically very different approach is used by Hwa and Yang (63). Instead of fragmenting hard partons directly, they define the parton contents of a jet (initiated by a hard parton), the so-called shower distributions. They are given by non-perturbative splitting functions $S_{ij}(z)$ which describe the probability to find a parton of flavor j with momentum fraction z in a jet originating from a hard parton i. The parton content of a single jet can then recombine and the resulting hadron spectrum has to match the result from jet fragmentation. Hwa and Yang fit the shape of the parton shower distributions to describe the known fragmentation functions for pions, protons and kaons (63). The power of this approach lies in the fact that the fragmentation part of the hadron spectrum is computed with the same formalism. It is then very natural to also coalesce shower partons with thermal partons (55).

The HY approach is also well-suited to discuss medium corrections to fragmentation in much more dilute systems like $p + A$ collisions (64). It was found that the hadron-dependent part of the Cronin effect in $d + Au$ collisions at RHIC can be attributed to coalescence of jet partons with soft partons from the underlying event. A more rigorous definition of parton showers and a discussion of the scale dependence can be found in the work by Majumder, Wang and Wang (65).

2.4 Elliptic Flow

In the momentum-space formulation it is straight forward to predict the particle-type dependence of the elliptic flow v_2 of hadrons (43) coming from coalescence. This derivation, repeated below, has been criticized as being too simplistic (66, 67). However, the scaling law holds numerically to very good approximation in

the GKL approach as well and we will see in the next section that the data from RHIC follows it with surprising accuracy. We return to discussing the criticism further in Sec. 4.

Let us assume that the elliptic flow of a set of partons a just before hadronization is given by an anisotropy $v_2^a(p_T)$ at mid-rapidity ($y = 0$). The phase space distribution of partons a can then be written in terms of the azimuthal angle ϕ as

$$f_a(\mathbf{p}_T) = \bar{f}_a(p_T)\left(1 + 2v_2^a(p_T)\cos 2\phi\right), \tag{13}$$

where odd harmonics are vanishing due to the symmetry of the system and higher harmonics are neglected. $\bar{f}$ is the distribution averaged over the azimuthal angle ϕ. A general expression for the elliptic flow of hadrons coalescing from these partons can be derived as a function of the parton elliptic flow. For a meson with two valence partons a and b and for small elliptic flow $v_2 \ll 1$ one has

$$
\begin{aligned}
v_2^M(p_T) &= \frac{\int d\phi \cos(2\phi)dN_M/d^2p_T}{\int d\phi dN_M/d^2p_T} \\
&\sim \int dx_a dx_b \Phi_M(x_a, x_b)\left[v_2^a(x_a p_T) + v_2^b(x_b p_T)\right].
\end{aligned}
\tag{14}
$$

The full expressions including corrections for large elliptic flow can be found in (49). In the case of a very narrow wave function in momentum space ($\alpha \to \infty$) this leads to the expression

$$v_2^M(p_T) = v_2^a(x_a p_T) + v_2^b(x_b p_T). \tag{15}$$

with fixed momentum fractions x_a and x_b ($x_a + x_b = 1$).

Thus for hadrons consisting of light quarks which exhibit the same elliptic flow before hadronization we arrive at a simple scaling law with the number of valence quarks n:

$$v_2^h(p_T) = nv_2^a(p_T/n). \tag{16}$$

This scaling law had originally been suggested by several authors after first indications for scaling had been found in data gathered at RHIC $(8, 12, 49, 68)$. Eq. (15) has also been used to estimate the elliptic flow of heavy quarks from measurements of heavy-light systems like D mesons $(69, 60)$. The treatment has also been extended to harmonics beyond the second order. Generalized scaling laws for the 4th and 6th order harmonics have been derived in Ref. (70).

2.5 Comparison of Approximations and Assumptions

The main features and the overwhelming success of the coalescence models of hadronization are shared by all the approaches discussed here. However, despite the agreement on the general properties and their ability to describe baryon and meson spectra, there are different approximations and assumptions involved. Some have already been mentioned in the previous paragraphs. We want to discuss some additional points in more detail here.

One important difference not mentioned thus far is the mass of the quarks in the parton phase. GKL and FMNB use effective masses that are roughly of the size of the constituent quark masses in the hadrons formed (i.e. $m_{u,d} \approx 300$ MeV, $m_s \approx 475$ MeV). This can be justified by the fact that coalescence does not explicitly include all the interactions. A part of the non-perturbative physics is encoded in the dressing of quarks, leading to a finite mass. This is also consistent with the requirement of (at least approximate) energy conservation. Furthermore quasi-particle descriptions of the thermodynamics properties of the quark gluon plasma estimate thermal masses of about 400 MeV $(71, 72)$. However, the exact relation between masses in a chirally broken phase and thermal masses above T_c remains to be an open question. On the other hand, in the HY approach

massless quarks are assumed. For the phenomenology at intermediate momenta, $p > m$, masses do not play a too important role, wherefore a good description of measured spectra can be obtained with both assumptions.

The missing position-space information is a weakness of the FMNB and HY implementations. In principle, very complex space-momentum correlations might exist in the parton phase before hadronization, and they might be important to describe elliptic flow in an appropriate fashion (66, 67, 68). However, in the actual GKL computations, the spatial distribution is taken to be uniform, similar to the assumption used in pure momentum-space implementations. The only space-momentum correlation in GKL are those coming from radial flow and no systematic tests of more complicated space-momentum correlations are available in this formalism.

On the other hand, GKL has the advantage to be able to easily accommodate resonance formation and decay (53). Direct observations of baryon anomaly and elliptic flow scaling are available only for stable hadrons so far. But stable hadrons can contain a large feed-down contribution from resonance decays, especially the pions (73, 74, 75). At intermediate p_T the role of resonance decays is somewhat reduced, which justifies neglecting resonances as done by FMNB and HY. The violation of the v_2 scaling law is generally mild, which emphasizes this point. However, GKL shows that by including resonance decays both p_T-spectra and v_2 exhibit better agreement with data towards lower p_T (76). A schematic study of the elliptic flow of resonances themselves has been conducted in the FMNB formalism. It was found that elliptic flow is sensitive to the amount of resonances formed in the hadronic phase vs resonances emerging directly from hadronization (77).

We summarize the main differences among the approaches discussed in this section in Table 1.

3   Data from Elementary and Heavy-ion collisions

In this section we compare various coalescence model calculations to the available data and present predictions for future measurements. We start with single inclusive measurement, in particular spectra, hadron ratios and nuclear modification factors. We then proceed to discuss elliptic flow, particle correlations, and fluctuations. While all of these observables naturally focus at RHIC data taken during runs at $\sqrt{s} = 62.4$, 200 GeV, we conclude by giving an overview of the situation at different energies.

3.1   Hadron Spectra and Baryon to Meson Ratios

In Fig. 4 we show results from a coalescence model calculation of identified particle spectra using the FMNB method (49). The spectra of neutral pions, kaons, protons and hyperons for central Au+Au collisions at 200 GeV are compared to date from RHIC (38, 41). The salient features of the spectra are an exponential fall-off at intermediate p_T with a transition to a harder power-law shape at higher p_T, as we predicted above. The transition from an exponential shape to a power-law shape happens at a higher p_T for baryons than it does for mesons, again in accordance with the predictions from simple underlying principles.

Fig. 5 shows two baryon-to-meson ratios: anti-protons vs pions (left panel), and Λ-baryons vs K_S^0-mesons (right panel). Results from the GKL model for $\overline{p}/\pi^-$ (53) and $\Lambda/2K_s^0$ (78) and from the FMNB model (49, 79) are compared to data from RHIC. Both calculations describe a baryon enhancement at intermediate

p_T that diminishes until the spectra are dominated by fragmentation at higher p_T. The GKL model appears to provide a better description of the data but a comprehensive analysis of the systematic uncertainties in the models has not been presented. More baryon-to-meson ratios can be found in Fig. 12.

3.2 Elliptic Flow and Quark Number Scaling

Early identified particle measurements at RHIC showed that for $p_T < 1$ GeV/c, v_2 at a given p_T is smaller for more massive hadrons and that when plotted vs $m_T - m_0$, the v_2 for different species fell on a single curve. With higher statistics, measurements began to reveal that at higher p_T the mass ordering breaks and more massive baryons exhibit larger v_2 values (80, 81). This observation led to the first speculation about hadron formation from coalescence and scaling of v_2 with quark number. These speculations then culminated in detailed calculations that we show in this subsection.

Fig. 6 shows data on v_2 scaled by the number n of valence quarks in a given hadron as a function of p_T/n for several species of identified hadrons at $\sqrt{s_{NN}}$ = 200 GeV (40, 82). A polynomial function has been fit to the scaled values of v_2. To investigate the quality of agreement between hadron species, the data from the top panel are scaled by the fitted polynomial function and plotted in the bottom panel. Best agreement with scaling is found for $p_T/n > 0.6$ GeV/c. Below that, hadron v_2/n is ordered by mass.

By combining $m_T - m_0$ scaling and quark number scaling, one can achieve a better scaling across the whole momentum range (42). Fig. 7 shows v_2/n vs $(m_T - m_0)/n$ for several species of mesons and baryons. The scaling at low $m_T - m_0$ holds with an accuracy of 5-10%. At higher $m_T - m_0$, a violation of the

simple scaling becomes apparent. In the bottom panel of Fig. 7, v_2/n is scaled by a polynomial fit to the meson v_2/n only. The ratio of the data to the fit shows that baryon v_2/n tends to lie below the meson v_2/n.

The break-down of the simple quark number scaling was predicted by several authors (76, 66, 67, 68, 69) on the grounds of numerous arguments On the other hand, no clear consensus has emerged on whether the kinetic energy scaling at intermediate p_T is just a consequence of p_T scaling (since $m_T - m_0 \rightarrow p_T$ with increasing p_T) or whether it offers genuine new insights. Fig. 8 presents a comparison of data with the predictions for scaling violations. The bottom panel shows the ratio $(B - M)/(B + M)$, where B is v_2/n for baryons and M is v_2/n for mesons. In this figure K_S^0 serve as an example for mesons and $\Lambda + \overline{\Lambda}$ for baryons. The pion and proton v_2 have been shown to be, within errors, consistent with the v_2 of K_S^0 and $\Lambda + \overline{\Lambda}$, respectively (84, 83). Two predictions for scaling violations are shown as well.

Three possible sources of violations of quark number scaling have been studied within the GKL and FMNB implementations. One source are realistic wave functions with finite width (as opposed to the limit $\alpha = 0$ needed for the derivation of scaling). Both theoretical curves shown in Fig. 8 use realistic wave functions (note however, that in GKL in addition the quarks don't have to be collinear). Another correction is expected from higher Fock states which should scale with higher weights $n + 1$, $n + 2$, etc. A study within the FMNB framework showed that while thermal spectra are almost unaltered, there are visible effects for v_2. However, those are numerically surprisingly small (51). Fig. 8 also contains a prediction including a 50% admixture of a state with one additional gluon. A third breaking of scaling is expected from resonance decays studied in (76).

Those three effects cause the hadron v_2/n to fall below the quark v_2 values. The reduction is larger for baryons so that the naive scaling is broken. The predicted violation (51,76) are in fairly good agreement with the data (84). For $p_T > 2 - 2.5$ GeV hadronization should be dominated by fragmentation, hence the $(B-M)/(B+M)$ should relax to the value -0.2 if baryons and mesons from fragmentation have equal v_2 and depend only weakly on p_T. The fragmentation contribution is not included in either theoretical calculation in Fig. 8. We discuss further arguments against v_2-scaling in Sec. 4.2.

The RHIC program has also confirmed, for the first time, the existence of non-vanishing higher azimuthal anisotropies, beyond elliptic flow (85). The existence of a sizable fourth harmonic $v_4 = \langle \cos(4\phi) \rangle$ had been anticipated in hydrodynamic calculations (86). Coalescence predictions for the relative v_4 of baryons and mesons provide further checks for the recombination picture. Such relations have been first worked out (70). Concrete computations were later performed in the GKL model (78), where it was found that the difference between baryon and meson v_4 is much more pronounced than for v_2. This might lead to valuable constraints for coalescence models in future high-statistics runs at RHIC. Fits have been performed for identified particle v_4 from 62.4 GeV Au+Au collisions. These studies report good agreement with data for quark v_4 approximately 2× quark v_2^2 (83).

3.3   Heavy Quarks

Coalescence has also been applied to study hadrons involving heavy quarks, in particular for D and B mesons (60,87,88). Such studies have attracted increasing interest due to the surprisingly strong interaction of heavy quarks in the medium

first seen in the R_{AA} (92,91) and v_2 of single electrons coming from semi-leptonic decays of D and B mesons. While the main challenge is to understand the origin of this strong interaction with the medium, the hadronization mechanism plays a significant role in the interpretation of the data (89, 90). We show this in Figs. 9 and 10 where the R_{AA} and the v_2 of single electrons from semi-leptonic decays is shown together with experimental data from PHENIX and STAR (91, 92). Comparing the solid (coalescence plus fragmentation) and dashed band (fragmentation only) one notices a significant effect from coalescence. It manifests itself in an increase of both R_{AA} and v_2 up to $p_T \sim 3$ GeV/c for single electrons (which corresponds to about $p_T \sim 7$ GeV at the meson level. The effect is crucial because coalescence reverses the usual correlation between R_{AA} and v_2 and so allows for a better agreement with the data. We note that the non-photonic electron spectrum can also be effected by coalescence if the Λ_c/D ratio is enhanced in Au+Au collisions compared to p+p collisions (93). This is because the branching ratios to electrons are much smaller for charm baryons than for charm mesons.

An important development is the impact of coalescence on the physics of quarkonia in a quark-gluon plasma. Even though coalescence has been applied to the J/Ψ for many years, the present implementations can be used to check not only the yield but also the spectra and the elliptic flow as a function of transverse momentum. This makes it possible to perform consistency checks between the spectra observed for open charm mesons and for J/Ψs. Such studies will be of particular interest at LHC where the J/Ψ should be dominated by regeneration in the plasma (94, 95). In addition, recent studies have found that even if the binding of a J/Ψ is screened in a quark-gluon plasma, the spectral function

still exhibits correlations above those expected for free quarks (96). These residual correlations may have important implications at hadronization that can be studied in future recombination calculations.

3.4 Particle Correlations and Fluctuations

Single particle observables and elliptic flow motivated coalescence models and were a success story throughout the history of RHIC data taking. Later, measurements of hadron correlations challenged this picture. At RHIC it has been possible to measure the correlation between a trigger particle with momentum p_T^{trig} and an associated particle with momentum p_T, typically smaller than p_T^{trig}. The experimental observable is usually the associated yield, which is the yield of correlated pairs divided by the trigger yield. Associated yields have been measured as a function of relative azimuthal angle $\Delta\phi$, and both trigger and associated p_T (97,98). This observable is ideal to detect correlations typical for jets. Jets give signals at $\Delta\phi = 0$ (near-side jet) and $\Delta\phi = \pi$ (away-side jet). It was at first very surprising that such jet-like correlations were found with both trigger and associated p_T in the recombination domain below 4 to 6 GeV/c.

It was then quickly realized that correlations among hadrons in this kinematic regime can come about through two mechanisms. First, mixed soft-hard recombination or thermal-shower recombination naturally leads to correlated hadrons. This was first explored by Hwa and Yang (99). A shower parton coalescing to become part of a hadron at intermediate p_T will provide a correlation of this hadron with all those hadrons coming from fragmentation of the same jet, or the associated away-side jet.

A second possibility was pointed out in a work by Fries, Müller and Bass in

an extended FMNB framework (62, 100, 101). They showed that any residual correlations in the tail of the bulk parton distribution automatically leads to correlations among the coalescing hadrons. To prove this point they introduced weak 2-particle correlations as corrections to the usual factorization ansatz for the multi-parton Wigner functions, e.g.

$$W_{ab}(p_a, p_b) = f_{\text{th}}(p_a)f_{\text{th}}(p_b)\left(1 + C_{ab}(p_a, p_b)\right) \tag{17}$$

for two partons a, b. Under these specific assumptions they obtained correlations for the coalescing hadrons that are amplified by the product of valence quarks numbers (4, 6 and 9 for meson-meson, baryon-meson and baryon-baryon pairs resp.), similar to the enhancement of elliptic flow by the number of valence quarks. While it is not clear that the specific assumptions (very weak 2-particle correlations) hold at RHIC a reasonable result for associated yields as a function of centrality was obtained.

Fig. 11 shows the associated yield of near-side hadrons for trigger baryons (right panel) and trigger mesons (left panel) calculated in (62) together with PHENIX results from (102). A scaling law for correlations between different pairs of hadron species has not been observed in data so far. This is compatible with the fact that correlations from jet fragmentation are strong and have to be added even at intermediate p_T, even though fragmentation is suppressed in single inclusive observables at the same p_T (62). The authors of this study argued that the phase space relevant for recombination at intermediate momentum is not necessarily completely thermalized. Rather, remnants of quenched jets, so-called hot spots could be an important component, leading to some residual jet-like correlations among partons through simple momentum conservation. Independent of the modeling in detail, one can conclude that recombination has been shown to be

compatible with measurable correlations at intermediate p_T.

Charge fluctuations (103) have been shown to be consistent with the recombination process as well. They are considered to be a good probe for QGP formation. General expectations from coalescence are in fairly good agreement with data (105, 104). A recent, more specific study shows that consistency with coalescence is obtained if the number of quarks and antiquarks is approximately $dN/dy \cong 1300$ for central collisions (106). This is in agreement with the parton multiplicity estimated in the GKL implementation (53) and with the ALCOR model (107). This is a valuable consistency test for coalescence models.

3.5   Beam Energy Dependence

Most of the work published in the context of coalescence models focuses on Au+Au collisions at RHIC energies of 130 or 200 GeV. Of course, it is important to understand if the models can predict the correct behavior of observables, e.g. baryon-to-meson ratios, as a function of collision energy $\sqrt{s}$. Before the low energy Au+Au run at RHIC with $\sqrt{s} = 62$ GeV was completed, a prediction was presented within the GKL approach, utilizing a simple extrapolation of the model parameters (108). It was found that the p/π ratio increases compared to $\sqrt{s} = 200$ GeV while the $\overline{p}/\pi$ ratio decreases. This is exactly what was measured when the lower energy data was analyzed (109). The predictions for scenarios with and without coalescence are shown together with the data in Fig. 12. The data are clearly favoring the scenario with quark coalescence. The discrepancy found for $\overline{p}/\pi$ at $p_T > 7$ GeV might be due to the poor knowledge of the identified proton fragmentation function (108).

On the other side, results from heavy ion collisions at much larger energies will

soon become available. The Large Hadron Collider LHC at CERN will collide Pb ions at a center of mass energy of $\sqrt{s} = 5.5$ TeV per nucleon-nucleon pair. This will lead to QGP fireballs with much higher temperatures. On the other hand one can also predict that the number of hard processes increases tremendously due to the rising gluon distribution at small Bjorken-x. Naively, one would expect the window in p_T where coalescence is dominating to increase. However, the estimates for this region depend delicately on the radial flow (which pushes the coalescing hadrons to higher p_T) and jet quenching (which leads to less fragmented hadrons at high p_T).

Possible scenarios have been explored in the FMNB framework using different assumptions for the radial flow (110). These estimates are shown in Fig. 13. Recently, a more systematic study of elliptic flow as a function of collision energy was published (111).

4   Challenges and Outlook

The RHIC program has provided remarkable evidence that coalescence of quarks is the dominating mechanism for hadronization from a deconfined plasma. Nonetheless, some problems remain unsolved and several new questions are raised by the formalism itself. E.g. it is appealing to apply recombination at low momenta where the phase space is more dense. Some of these problems have been touched upon briefly in previous sections. We will discuss them in more detail below.

4.1   Energy and Entropy

A basic issue that involves all approaches based on instantaneous projection is that of energy conservation. The underlying kinematics of the projection is ef-

fectively $2 \to 1$ and $3 \to 1$, which makes it impossible to conserve 4-momentum. This is somewhat mediated at intermediate transverse momenta, $p_T > m$, where the kinematics is essentially collinear and violations of energy conservation are suppressed by factors m/p_T or k_T/p_T where k_T is the intrinsic transverse momentum of a parton inside the hadron. In principle, this is not really acceptable, since the formalism should be easily extendable to low p_T where collinearity is missing. In fact, a smooth matching with bulk coalescence models like ALCOR should be possible, which describe multiplicities and related observables at low p_T successfully (30,112). Interestingly, a naive extension of the GKL approach to low momenta does not lead to striking disagreement with the experimental data (53,89). However from the theoretical point of view the issue of imperfect energy conservation is clearly unsatisfying.

Energy conservation has to be achieved through interactions with the surrounding medium. Naturally, approximations to this multi-particle dynamics have to be applied to make the problem tractable. One way is to introduce an effective mass distribution for the quarks as a way to incorporate some in-medium effects (113). This allows to enforce both momentum and energy conservation and one finds fairly good agreement with data for p_T-spectra.

A promising new and very powerful approach has recently been developed by Ravagli and Rapp (RR) (48). They replace the instantaneous projection of quark states onto hadron states by a procedure which solves the Boltzmann equation for an ensemble of quarks which are allowed to scatter through hadronic states. Thus the hadrons are given through cross sections with a certain width. This implementation naturally conserves 4-momentum. Ravagli and Rapp find quite good agreement with data for p_T-spectra. They also confirm v_2 scaling (neglecting

position-momentum correlations as the other approaches). However, they find that kinetic energy scaling (v_2 vs $m_T - m_0$) is in even better agreement with experimental data, cf. Fig. 7. The RR formalism with energy conservation is the only one really suited to address the question of kinetic energy scaling.

A related issues is entropy conservation. Coalescence through instantaneous projection seems to reduce the number of particles by about a factor two, which understandably rises the question whether the second law of thermodynamics is violated. However, strictly speaking this formalism should only be applied at intermediate p_T where only a small fraction of the total particle number ($< 2\%$) is located. Furthermore, the situation is much less dire if resonance production is taken into account which significantly increases the number of hadrons in the final state (89, 53). Entropy depends not only on the number of particles, but also on the degeneracies in both phases and on the masses.

In addition one should also take into account the interaction among quarks. It has been shown for an isentropically expanding fireball, using the lattice equation of state, that the evolution of the effective number of particles reduces significantly around the crossover temperature (114). This could help to solve the entropy problem inherent to instantaneous quark coalescence, as also pointed out by Nonaka and collaborators (106). However, it is still a challenge to find a consistent approach to conserve both energy and conserve or increase entropy, together with a good description of single particle spectra and elliptic flow for both low and intermediate p_T.

4.2 Space-Momentum Correlations

An important open question is the relation between space-momentum correlations and v_2 scaling. The valence quark number scaling of elliptic flow was derived in a pure momentum-space picture. This means that the scaling has been explicitly proven only if the coalescence probability is homogeneous in space. GKL have gone one step beyond by including correlations of radial flow with the radial coordinate r. They find that scaling still holds to a good approximation with some small violations (53, 76, 89).

However, the situation could be very different if more realistic correlations of flow with the spatial azimuthal angle φ are taken into account. One should expect a strong correlation between the spatial azimuthal angle φ and the momentum azimuth ϕ. A detailed discussion of effects coming from space-momentum correlations can be found in the work by Pratt and Pal (66). They also map out a class of phase space distributions that lead to approximate scaling.

Parton cascade studies that calculate the time evolution of the phase space distributions find that approximate scaling between baryons and mesons still persists even if strong deviations of v_2 at the quark level are seen (67). However it is not clear how this depends on the freeze-out criteria, on the width of the wave functions and on the interplay with jet fragmentation. Another study on the effect of phase space distribution can be found in Ref. (68).

Small violations of v_2 scaling have been observed, but as discussed in detail in Sec. 3 they can be explained solely by wave function effects, resonance contributions and contributions from higher Fock states in hadrons (51, 108, 115). If the scaling feature were accidental and strongly dependent on details of the phase space distribution, the very different dynamical evolution at LHC might lead to

much stronger scaling violations there. A better understanding of HBT measurements could also supply fundamental information on this issue. It would also be interesting to see how realistic phase space correlations will fare in a dynamical coalescence model like the RR formalism.

4.3 Outlook

Quark coalescence models for heavy ion collisions have reached a certain level of maturity, but it has also become clear that there are limitations. We hope that several issues will attract attention in the future.

Within the established projection formalism several open questions can be addressed. A huge amount of data on 2- and 3-hadron correlations has been collected. While preliminary studies have shown that correlations are in principle compatible with recombination, a comprehensive effort to understand the data in a picture that contains jets, jet quenching, and coalescing partons at intermediate p_T still has to be developed. It would have to include a realistic microscopic modeling of the coupling between the medium and jets and how jet-like correlations can be conferred to the medium. A second issue concerns the role of resonance production. Little is know about the relative probabilities of coalescence into stable hadrons and unstable resonances. As we have seen above this is an important issue for multiplicities and entropy production as well as v_2 scaling violations (in particular for pions).

Dynamical transport implementations like the one developed by Ravagli and Rapp are very promising candidates to investigate more fundamental open questions. E.g., it would be straight forward to implement resonances and stable hadrons in a realistic fashion. Progress could be made on the issues of kinetic

energy vs transverse momentum scaling of v_2, the role of space-momentum correlations for elliptic flow scaling, and entropy production. There is also a need to explore dynamical coalescence coupled to realistic transport models for the parton and hadron phase.

There is a list of more profound questions which we have not touched upon yet at all. Coalescence of particles can be found in systems which do not exhibit confinement (e.g. in plasmas of electrons and protons). Confinement does not play a big role in any of the current implementations of coalescence. (In parton cascades, non-coalescing partons are usually fragmented, the only tribute to the fact that there are no free partons allowed in the vacuum.) Nevertheless there should be a fundamental difference between confining and non-confining theories. Transport implementations need to explore this difference in the future.

It is also not clear what the role of chiral symmetry breaking during the coalescence process is. Most implementations give constituent-like masses to the quarks, but no direct connection to chiral or thermal masses is made. Unfortunately the current observables do not seem to be sensitive to the nature of the quark masses. We would hope that improved implementations together with new high-statistics data might allow us to address this question.

5 Conclusions

The first stage of the RHIC program has provided clear evidence that hadronization at transverse momenta of several GeV/c is modified when compared to $p + p$ collisions in the light quark sector. The available data is only compatible with a hadronization process through coalescence of quarks. The baryon enhancement and the robust scaling of the elliptic flow with the number of valence quarks are

signatures which rule out other explanations.

We have presented a comprehensive overview of the available coalescence models, which are mostly based on an instantaneous projection of quark states onto hadron states. On the other hand, dynamical coalescence uses scattering of quark into hadron states in a transport approach. We have discussed some of the weaknesses of current implementations and how the field might evolve in the future.

Let us conclude by discussing a statement that has naturally arisen after coalescence models had been applied to RHIC. It was pointed out again and again that coalescence might be the most convincing argument to show that confinement takes place at RHIC and a quark gluon plasma is indeed formed. The argument used relies on the fact that elliptic flow v_2 is a collective effect (coming from the hydrodynamic expansion due to pressure gradients), and that this collectivity seems to happen on the parton level, leading to a universal elliptic flow for quarks just above T_c. In other words, elliptic flow of hadrons at intermediate p_T did not emerge from hadronic interactions.

This is indeed very remarkable and it is a strong argument for deconfinement. All signatures for deconfinement use indirect arguments and need some kind of theoretical input to reach this conclusion. Coalescence, and in particular the v_2 scaling, appear to be convincing because almost no additional assumptions seem to be needed. We hope that this argument is solidified with future improvements in our understanding of data and of the mechanism of recombination.

6 Acknowledgments

LITERATURE CITED

1. Karsch F. *Lect. Notes Phys.* 583:209 (2002)

   Cheng M, et al. *Phys. Rev. D* 74:054507 (2006)

2. Fodor Z, Katz SD. *JHEP* 0203:014 (2002)

   Fodor Z, Katz SD. *JHEP* 0404:050 (2004)

3. Adams J, et al (STAR Collaboration). *Nucl. Phys.* A757:102 (2005)

   Adcox K, et al (PHENIX Collaboration). *Nucl. Phys.* A757:184 (2005)

4. Gyulassy M, McLerran L. *Nucl. Phys.* A750:30 (2005)

5. Adler SS, et al (PHENIX Collaboration). *Phys. Rev. Lett.* 91:172301 (2003)

6. Adams J, et al (STAR Collaboration). *Phys. Rev. Lett.* 92:052302 (2004)

7. Adams J, et al (STAR Collaboration). *Phys. Rev. C* 72:014904 (2005)

8. Voloshin SA. *Nucl. Phys.* A715:379 (2003)

9. Hwa RC, Yang CB. *Phys. Rev. C* 67:064902 (2003)

10. Fries RJ, Muller B, Nonaka C, Bass SA. *Phys. Rev. Lett.* 90:202303 (2003)

11. Greco V, Ko CM, Levai P. *Phys. Rev. Lett.* 90:202302 (2003)

12. Molnar D, Voloshin SA. *Phys. Rev. Lett.* 91:092301 (2003)

13. Vance SE, Gyulassy M, Wang XN. *Phys. Lett.* B443:45 (1998)

    Vitev I, Gyulassy M. *Phys. Rev. C* 65:041902 (2002)

    Pop VT, et al. *Phys. Rev. C* 70:064906 (2004)

14. Huovinen P, et al. *Phys. Lett.* B503:58 (2001)

    Kolb PF, *AIP Conf. Proc.* 698:694 (2004)

15. Kolb PF, Heinz UW. 2004. In *Quark Gluon Plasma 3*. ed. RC Hwa, XN
    Wang, 634. Singapore: World Scientific. preprint *arXiv:nucl-th/0305084*

16. Hirano T, Nara Y. *Phys. Rev. C* 69:034908 (2004)

17. Chernyak VL, Zhitnitsky IR. *Nucl. Phys.* B246:52 (1984)

Brodsky SJ, Lepage GP. *Adv. Ser. Direct. High Energy Phys.* 5:93 (1989)

18. Aitala EM, et al (E791 Collaboration), *Phys. Rev. Lett.* 86:4768 (2001)

19. Bakulev AP, Mikhailov SV, Stefanis NG. *Phys. Lett.* B508:279 (2001). erratum *Phys. Lett.* B590:309 (2004)

20. Collins JC, Soper DE. *Nucl. Phys.* B194:445 (1982)

21. Owens JF. *Rev. Mod. Phys.* 59:465 (1987)

22. Collins JC, Soper DE, Sterman G. *Adv. Ser. Direct. High Energy Phys.* 5:1 (1988). preprint *arXiv:hep-ph/0409313*

23. Kniehl BA, Kramer G, Potter B. *Nucl. Phys.* B582:514 (2000)

    S. Albino, B. A. Kniehl and G. Kramer, *Nucl. Phys.* B725:181 (2005)

24. Das KP, Hwa RC. *Phys. Lett.* B68:459 (1977). erratum *Phys. Lett.* B73:504 (1978)

25. Adamovich M, et al (WA82 Collaboration). *Phys. Lett.* B305:402 (1993)

26. Aitala EM, et al (E791 Collaboration). *Phys. Lett.* B371:157 (1996)

27. Braaten E, Jia Y, Mehen T. *Phys. Rev. Lett.* 89:122002 (2002)

28. Gupt C, Shivpuri RK, Verma NS, Sharma AP. *Nuovo Cim. A* 75:408 (1983)

    Lopez JA, Parikh JC, Siemens PJ. *Phys. Rev. Lett.* 53:1216 (1984)

29. Biro TS, Levai P, Zimanyi J. *Phys. Lett.* B347:6 (1995)

30. Biro TS, Levai P, Zimanyi J. *J. Phys. G* 28:1561 (2002)

31. Zimanyi J, Biro TS, Csorgo T, Levai P. *Phys. Lett.* B472:243 (2000)

32. Adler SS, et al (PHENIX Collaboration). *Phys. Rev. Lett.* 91:241803 (2003)

33. Adams J, et al (STAR Collaborations). *preprint arXiv:nucl-ex/0601042*

    Long H (STAR Collaboration). *J. Phys. G* 30:S193 (2004)

34. Adams J, et al (STAR Collaboration). *Phys. Rev. Lett.* 95:122301 (2005)

35. Adler SS, et al (PHENIX Collaboration). *Phys. Rev. Lett.* 91:182301 (2003)

36. Abreu P, et al (DELPHI Collaboration). *Eur. Phys. J. C* 17:207 (2000)

37. Alper B, et al (British-Scandinavian Collaboration), *Nucl. Phys.* B100:237 (1975)

38. Adams J, et al (STAR Collaboration). *Phys. Rev. Lett.* 98:062301 (2007)

39. Adams J, et al (STAR Collaboration). *Phys. Rev. C* 71:064902 (2005)

40. Abelev BI, et al (STAR Collaboration). *Phys. Rev. Lett.* 99:112301 (2007)

41. Abelev BI, et al (STAR Collaboration). *Phys. Rev. Lett.* 97:152301 (2006)

42. Afanasiev S, et al (PHENIX Collaboration). *Phys. Rev. Lett.* 99:052301 (2007)

43. Voloshin SA, Zhang Y. *Z. Phys. C* 70:665 (1996)

    Poskanzer AM, Voloshin SA. *Phys. Rev. C* 58:1671 (1998)

44. Ackermann KH, et al (STAR Collaboration). *Phys. Rev. Lett.* 86:402 (2001)

45. Adler C, et al (STAR Collaboration). *Phys. Rev. Lett.* 89:132301 (2002)

46. Molnar D, Gyulassy M. *Nucl. Phys.* A697:495 (2002). erratum *Nucl. Phys.* A703:893 (2002)

47. Baier R, Schiff D, Zakharov BG. *Ann. Rev. Nucl. Part. Sci.* 50:37 (2000)

    Gyulassy M, Vitev I, Wang XN, Zhang BW. preprint *arXiv:nucl-th/0302077*

48. Ravagli L, R. Rapp R. *Phys. Lett.* B655:126 (2007)

49. Fries RJ, Muller B, Nonaka C, Bass SA. *Phys. Rev. C* 68:044902 (2003)

50. Fries RJ, Muller B, Nonaka C, Bass SA. *J. Phys. G* 30:S223 (2004)

51. Muller B, Fries RJ, Bass SA. *Phys. Lett.* B618:77 (2005)

52. Fries RJ. *J. Phys. G* 30:S853 (2004)

53. Greco V, Ko CM, Levai P. *Phys. Rev. C* 68:034904 (2003)

54. Hwa RC, Yang CB. *Phys. Rev. C* 67:034902 (2003)

55. Hwa RC, Yang CB. *Phys. Rev. C* 70:024905 (2004)

56. Rapp R, Shuryak EV. *Phys. Rev. D* 67:074036 (2003)

57. Kapusta JI. *Phys. Rev. C* 21:1301 (1980)

58. Dover C, Heinz U, Schnedermann E, Zimanyi J. *Phys. Rev. C* 44:1636 (1991)

    Baltz AJ, Dover C. *Phys. Rev. C* 53: 362 (1996)

    Mattiello R, et al. *Phys. Rev. C* 55:1443 (1997)

59. Molnar D. *J. Phys. G* 30:S1239 (2004)

60. Greco V, Ko CM, Rapp R. *Phys. Lett.* B595:202 (2004)

61. Pal S, Pratt S. *Phys. Lett.* B578:310 (2004)

62. Fries RJ, Bass SA, Muller B. *Phys. Rev. Lett.* 94:122301 (2005)

63. Hwa RC, Yang CB. *Phys. Rev. C* 70:024904 (2004)

64. Hwa RC, Yang CB. *Phys. Rev. Lett.* 93:082302 (2004)

    Hwa RC, Yang CB, Fries RJ. *Phys. Rev. C* 71:024902 (2005)

65. Majumder A, Wang E, Wang XN. *Phys. Rev. C* 73:044901 (2006)

66. Pratt S, Pal S. *Nucl. Phys.* A749:268 (2005)

67. Molnar D. preprint *arXiv:nucl-th/0408044*

68. Greco V, Ko CM. preprint *arXiv:nucl-th/0505061*

69. Lin ZW, Molnar D. *Phys. Rev. C* 68:044901 (2003)

70. Kolb PF, Chen LW, Greco V, Ko CM. *Phys. Rev. C* 69:051901 (2004)

71. Levai P, Heinz U. *Phys. Rev. C* 57:1879 (1998)

72. Castorina P, Mannarelli M. *Phys. Lett.* B644:336 (2007)

73. Sollfrank J, Koch P, Heinz U. *Phys. Lett.* B252:256 (1990)

74. Hirano T. *Phys. Rev. Lett.* 86:2754 (2001)

75. Dong X, et al. *Phys. Lett.* B597:328 (2004)

76. Greco V, Ko CM. *Phys. Rev. C* 70:024901 (2004)

77. Nonaka C, et al. *Phys. Rev. C* 69:031902 (2004)

78. Greco V, Ko CM. *J. Phys. G* 31:S407 (2005)

79. Nonaka C, Fries RJ, Bass SA. *Phys. Lett.* B583:73 (2004)

80. Sorensen P (STAR Collaboration). *J. Phys. G* 30:S217 (2004)

81. Adare A, et al (PHENIX Collaboration). *Phys. Rev. Lett.* 98:162301 (2007)

82. Abelev BI, et al (STAR Collaboration). preprint *arXiv:0801.3466 [nucl-ex]*

83. Abelev BI, et al (STAR Collaboration). *Phys. Rev.* C 75:054906 (2007)

84. Sorensen PR. *Nucl. Phys.* A774:247 (2006)

85. Adams J, et al (STAR Collaboration). *Phys. Rev. Lett.* 92:062301 (2004)

86. Kolb PF. *Phys. Rev. C* 68:031902 (2004)

87. van Hees H, Greco V, Rapp R. *Phys. Rev. C* 73:034913 (2006)

88. van Hees H, Mannarelli M, Greco V, Rapp R. preprint *arXiv:0709.2884 [hep-ph]*

89. Greco V. *Eur. Phys. J. Special Topics* 155:45 (2008)

90. Greco V, van Hees H, Rapp R. *AIP Conf. Proc.* 964:232 (2007)

91. Adler SS, et al (PHENIX Collaboration). *Phys. Rev. Lett.* 96:032301 (2006)

92. Abelev BI, et al (STAR Collaboration). *Phys. Rev. Lett.* 98:192301 (2007)

93. Sorensen PR, Dong X. *Phys. Rev. C* 74:024902 (2006)

94. Grandchamp L, Rapp R. *Nucl. Phys.* A709:415 (2002)

95. Andronic A, Braun-Munzinger P, Redlich K, Stachel J. *Phys. Lett.* B652:259 (2007)

96. Mocsy A, Petreczky P. *Phys. Rev. Lett.* 99:211602 (2007)

   Mocsy A, Petreczky P. *Phys. Rev. D* 77:014501 (2008)

97. Adler C, et al (STAR Collaboration). *Phys. Rev. Lett.* 90:082302 (2003)

98. Adler SS, et al (PHENIX Collaboration). *Phys. Rev. C* 71:051902 (2005)

99. Hwa RC, Yang CB. *Phys. Rev. C* 70:054902 (2004)

100. Fries RJ. *J. Phys. G* 31:S379 (2005)

101. Fries RJ. *J. Phys. Conf. Ser.* 27:70 (2005)

102. Sickles A (PHENIX collaboration). *J. Phys. G* 30:S1291 (2004)

103. Jeon S, Koch V. *Phys. Rev. Lett.* 85:2076 (2000)

    Asakawa M, Heinz U, Muller B. *Phys. Rev. Lett.* 85:2072 (2000)

104. Bialas A. *Phys. Lett.* B532:249 (2001)

105. Mitchell J. *J. Phys G* 30:S819 (2004)

106. Nonaka C, Muller B, Bass SA, Asakawa M. *Phys. Rev. C* 71:051901 (2005)

107. Zimanyi J, Levai P, Biro TS. *Heavy Ion Phys.* 17:205 (2003)

108. Greco V, Ko CM, Vitev I. *Phys. Rev. C* 71:041901 (2005)

109. Abelev BI, et al (STAR Collaboration). *Phys. Lett.* B655:104 (2007)

110. Fries RJ, Muller B. *Eur. Phys. J. C* 34:S279 (2004)

111. Krieg D, Bleicher M. preprint *arXiv:0708.3015 [nucl-th]*

112. Csizmadia P, Levai P. *Acta Phys. Hung. A* 22:371 (2005)

113. Zimanyi J, Levai P, Biro TS. *J. Phys. G* 31:711 (2005)

114. Biro TS, Zimanyi J. *Phys. Lett.* B650:193 (2007)

115. Sorensen P. *J. Phys. G* 32:S135 (2006)
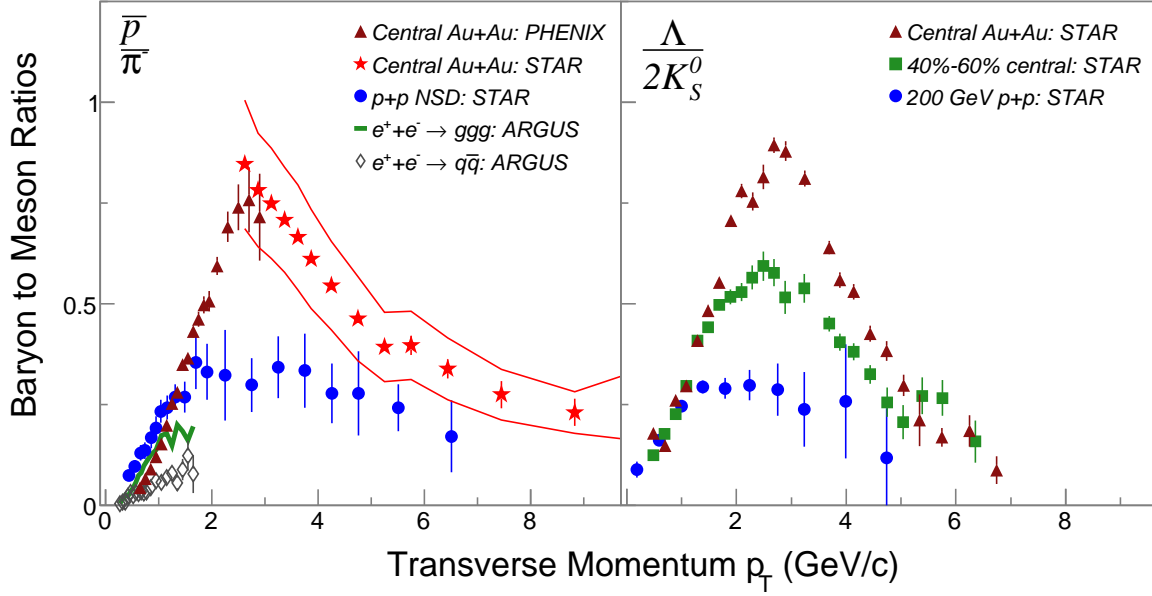
Figure 1: Left: $\overline{p}/\pi^-$ ratios measured in central Au+Au collisions at $\sqrt{s_{NN}} = 200$ GeV at RHIC, compared to measurements from $e^+ + e^-$ and $p + p$ collisions. Right: The ratio $\overline{\Lambda}/2K_S^0$ for central and mid-central Au+Au collisions at $\sqrt{s_{NN}} = 200$ GeV measured by STAR. The $\overline{p}/\pi^-$ ratio from p+p collisions from STAR is shown for comparison.

	GKL	FMNB	HY
Instantaneous coal.	Yes	Yes	Yes
Overlap integr.	Full 6-D	Long. momentum	Long. momentum
Soft-hard coal.	Yes	No	Soft-Shower
Massive quark	Yes	Yes	No
Resonances	Yes	No	No

Table 1: A summary of key differences between the most popular implementations: GKL = Greco, Ko, Lévai; FMNB = Fries, Müller, Nonaka, Bass; HY = Hwa, Yang.
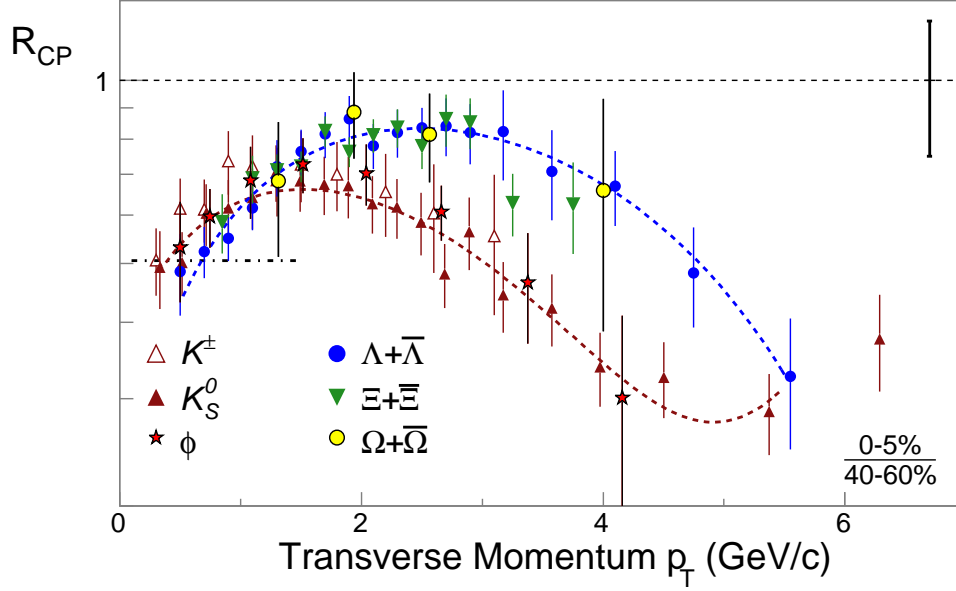
Figure 2: Nuclear modification factors (R_{CP}) for various identified particles measured in Au+Au collisions at $\sqrt{s_{NN}} = 200$ GeV by the STAR collaboration. The K_S^0 and $\Lambda + \overline{\Lambda}$ R_{CP} values demonstrate that strange baryon yields are enhanced in central Au+Au collisions compared to strange meson yields. Later, measurements of the ϕ, $\Xi + \overline{\Xi}$ and $\Omega + \overline{\Omega}$ showed that the rate of increase of the particle yields with collision centrality depended strongly on whether the particle was a baryon or meson with the mass dependence being sub-dominant: the baryon and meson R_{CP} values fall into two separate bands (indicated by lines to guide the eye) with the baryon R_{CP} larger than the meson R_{CP}.
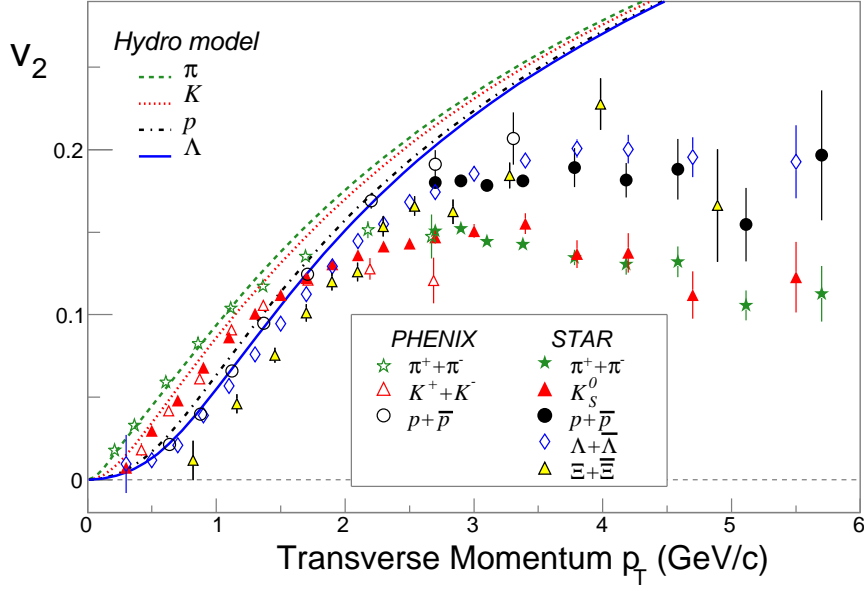
Figure 3: v_2 for a variety of particles from a minimum-bias sample of Au+Au collisions at $\sqrt{s_{NN}} = 200$ GeV measured by the STAR (6) and PHENIX (35) collaborations. Curves show the results from hydrodynamic model calculations (14). v_2 values also show that baryon production at intermediate p_T is enhanced in the in-plane direction, leading to larger baryon v_2. This observation is incompatible with expectation of v_2 coming from parton energy loss.
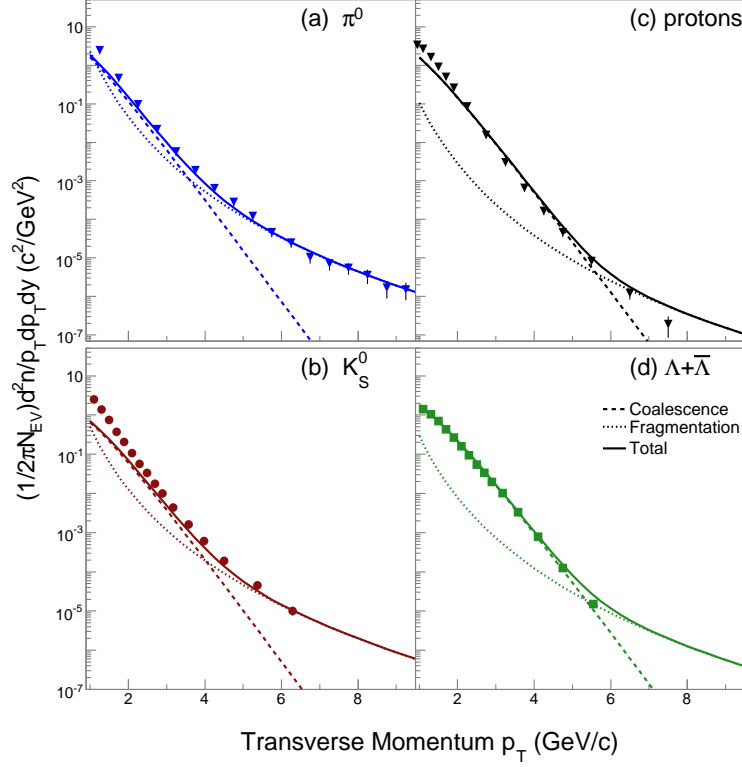
Figure 4: Hadron p_T-spectra at midrapidity from 200 GeV central Au+Au collisions. The curves show the recombination and fragmentation components of the spectra obtained in the FMNB formalism along with the total which compares well with the data.
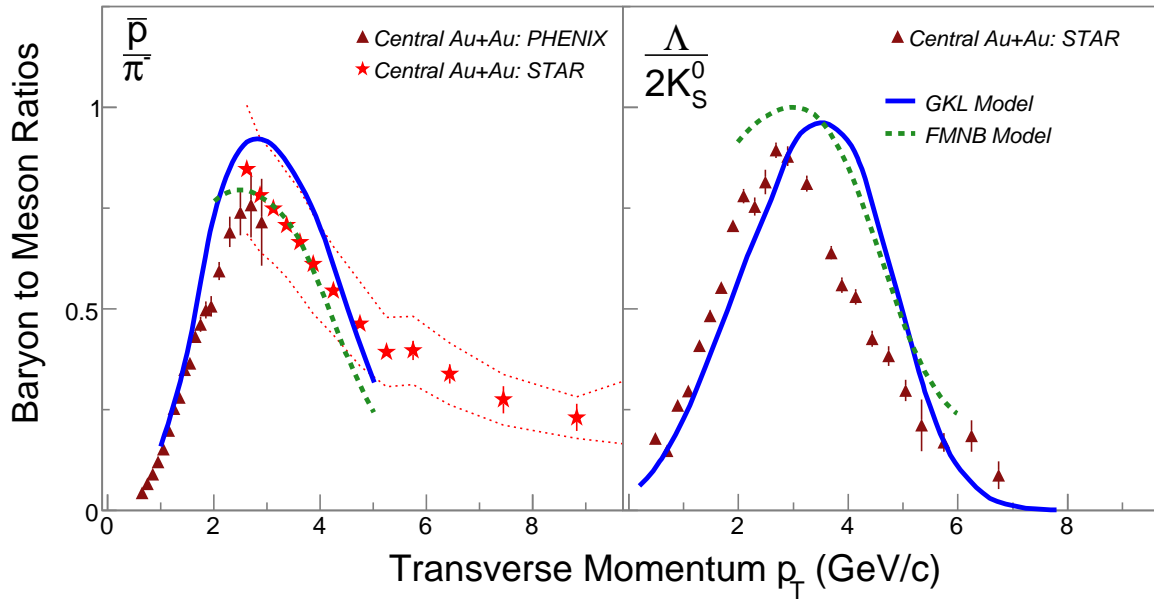
Figure 5: Ratios of baryon yields to meson yields for central Au+Au collisions at 200 GeV. The GKL and FMNB calculations for $\bar{p}/\pi^-$ (left) and $\Lambda/2K_s^0$ are compared to STAR and PHENIX data.
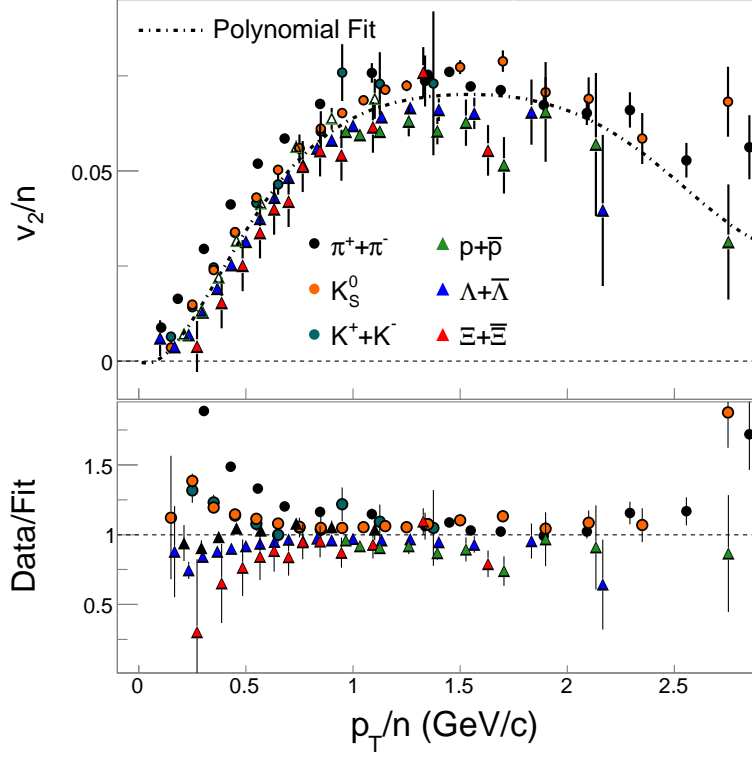
Figure 6: Top panel: The elliptic anisotropy parameter v_2 scaled by quark number n and plotted vs p_T/n. A polynomial curve is fit to all the data. The ratio of v_2/n to the fit function is shown in the bottom panel.
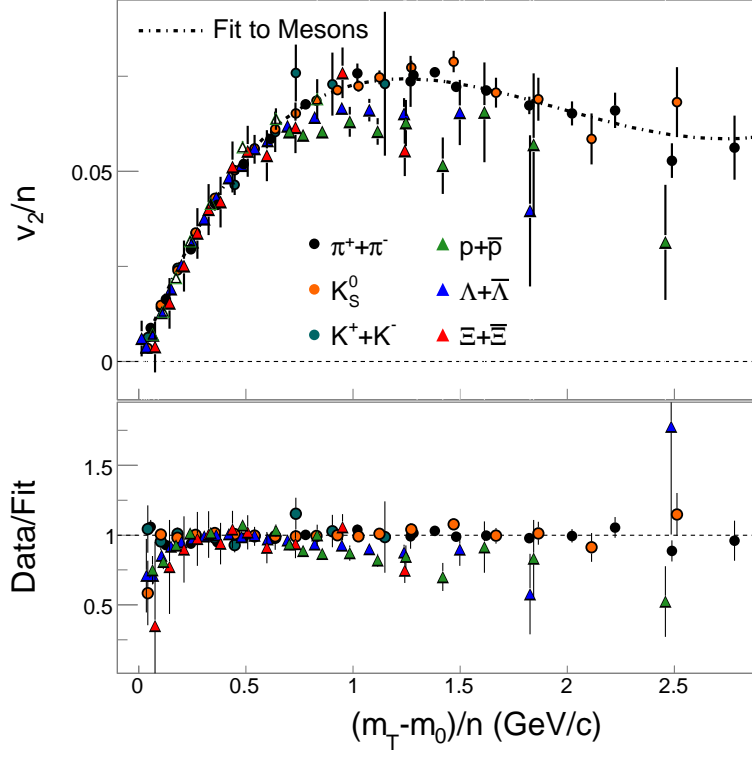
Figure 7: Quark number scaled elliptic flow vs $(m_T - m_0)/n$. In the low $m_T - m_0$ region, the scaling is improved by plotting vs $m_T - m_0$. All data is fit by a polynomial curve and the ratio of v_2/n to the fit function is shown in the bottom panel.
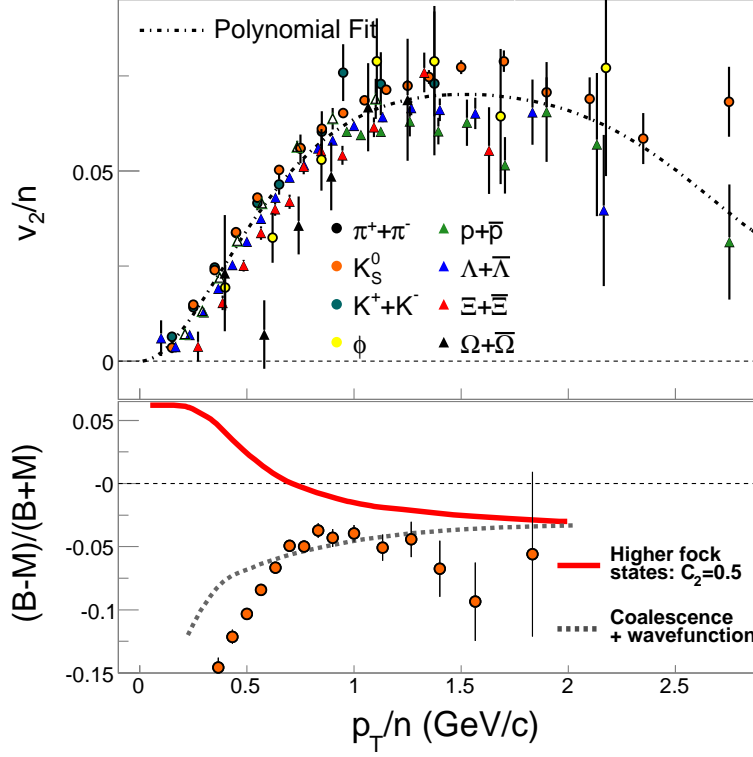
Figure 8: Top panel: Quark number scaled v_2 showing violation of ideal scaling. A polynomial is fit to all the available data. Bottom panel: The difference between quark number scaled baryon v_2 and quark number scaled meson v_2 divided by the sum: $(B - M)/(B + M)$. The ratio is formed using hyperons and kaons. The solid curve shows model predictions from FMNB using realistic wave functions and a 50% admixture of a higher Fock state containing an additional gluon. The dashed line shows calculations in the GKL model with realistic wave functions.
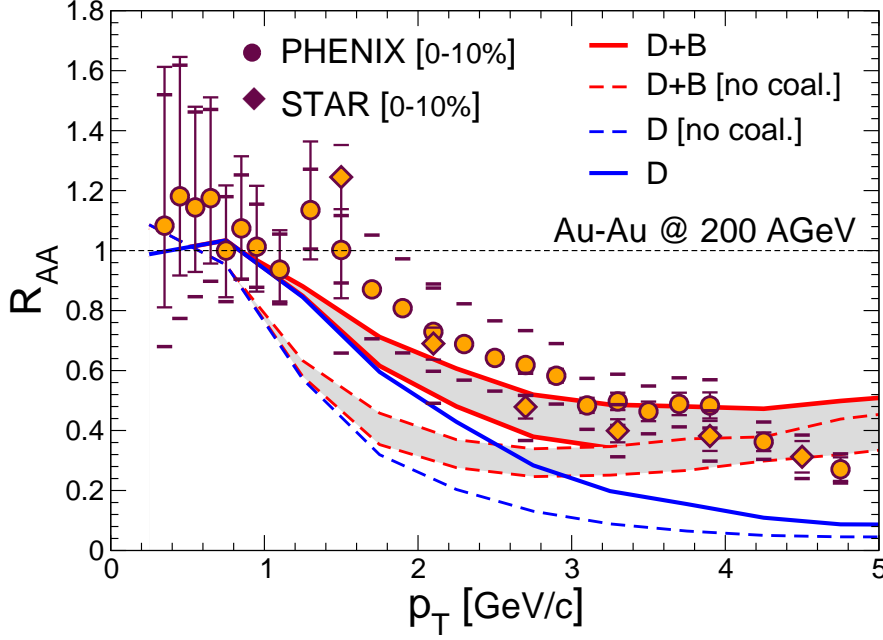
Figure 9: Nuclear modification factor R_{AA} of single electrons from semi-leptonic decays in Au+Au collisions at 200 GeV. The solid line represents the predictions from a coalescence plus fragmentation model (89) for electrons from D and B mesons (shaded bands) and from D mesons only (lines). The shaded band reflects the theoretical uncertainty in the heavy quark diffusion coefficients (87). The dashed lines are the results without coalescence. The data are taken from (91,92).
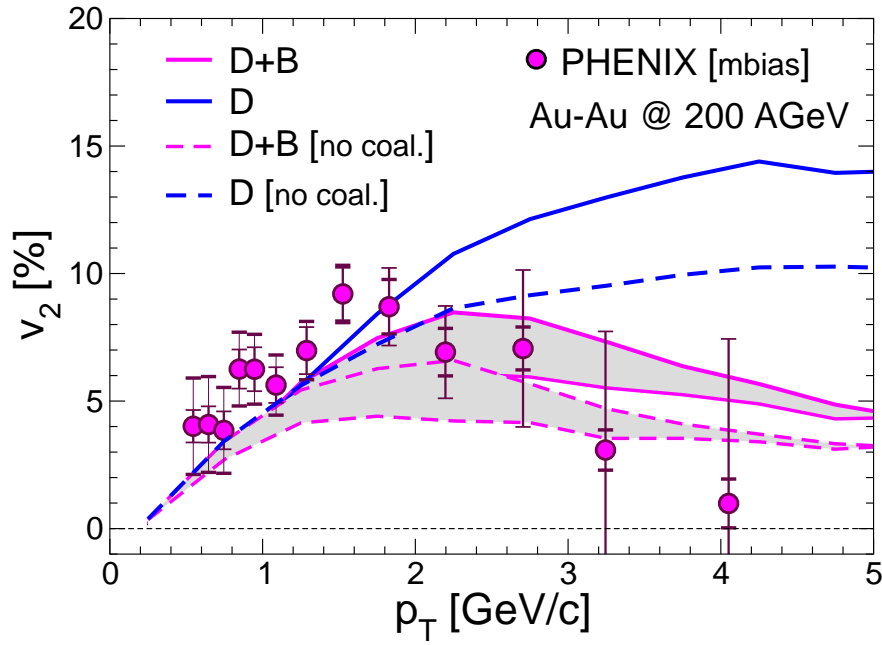
Figure 10: Elliptic flow v_2 of single electrons from semi-leptonic decays in Au+Au collisions at 200 GeV. The lines represent the same calculations as in Fig. 9. The data are taken from Ref. (91)
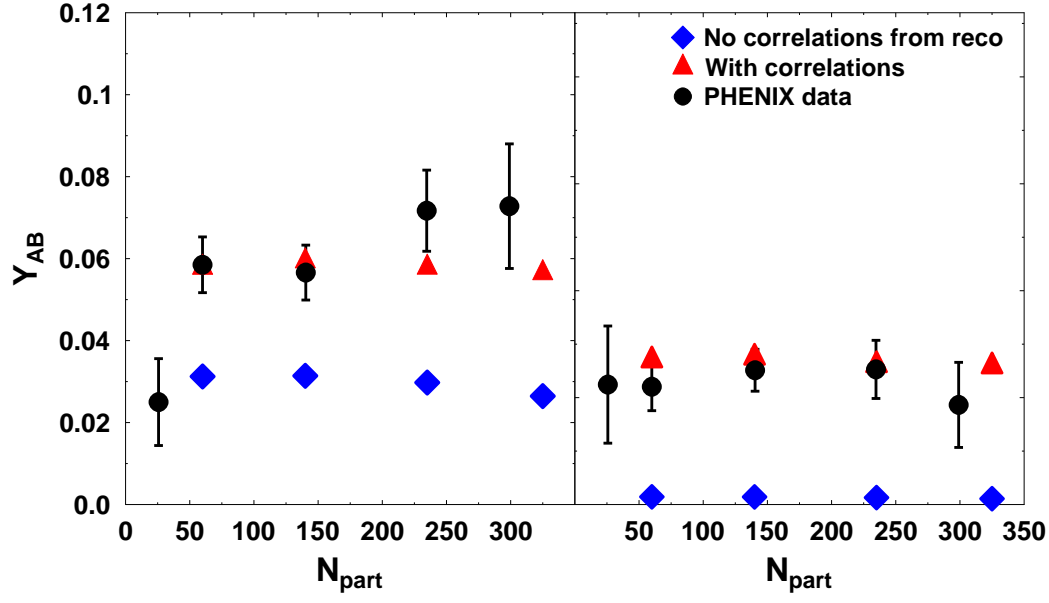
Figure 11: Associated hadron yields on the near-side as a function of number of participants for meson triggers (left) and baryon triggers (right) from (62). The diamonds represent the expected hadron correlations if fragmentation is the only source of correlations and recombination is correlation-free. Triangles show the same calculation with small 2-particle correlations among coalescing partons.
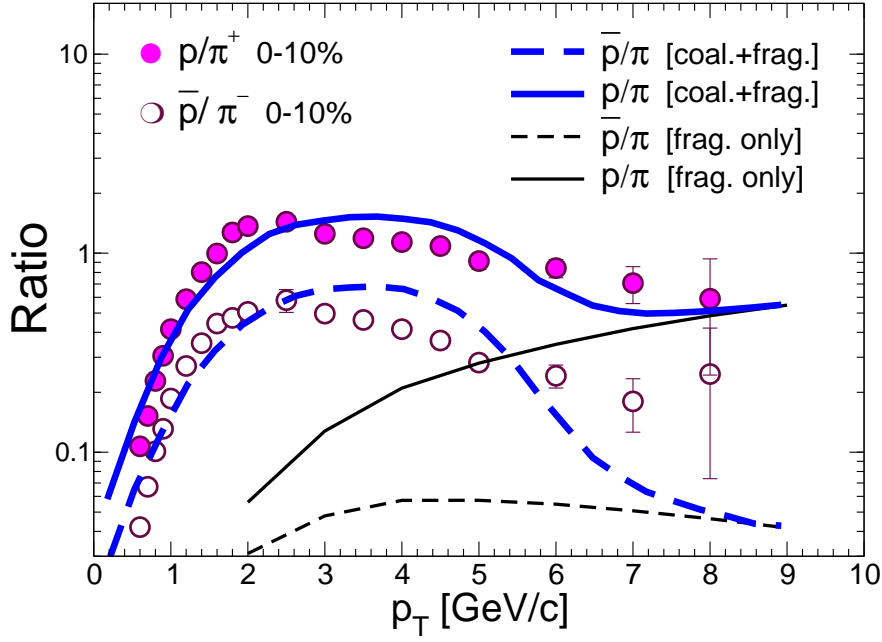
Figure 12: p/π^+ ratio and $\overline{p}/\pi^-$ ratio in central Au+Au collisions at 62.4 GeV. The predictions of the GKL model (coalescence plus fragmentation) (108) are shown by thick solid lines for p/π^+ and by thick dashed lines for $\overline{p}/\pi^-$; the prediction from fragmentation only are the corresponding thinner lines. The data from STAR are taken from Ref. (109)
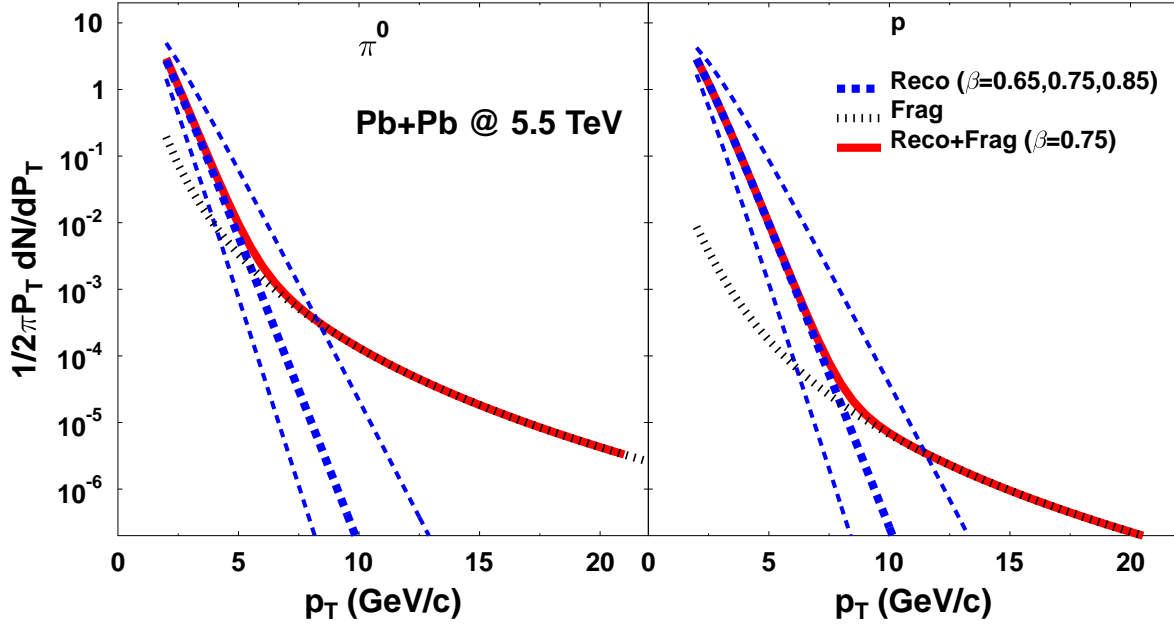
Figure 13: Predictions for π^0 (left) and proton (right) spectra in central Pb+Pb collisions at LHC using radial flow parameters $\beta = 0.65, 0.75$ and 0.85 resp. The larger the radial flow the more the recombination region extends to higher p_T, possibly up to 10 GeV/c (from (110)).